ACS Catalysis

pubs.acs.org/acscatalysis

Research Article

Computational Redesign of an ω-Transaminase from *Pseudomonas jessenii* for Asymmetric Synthesis of Enantiopure Bulky Amines

Qinglong Meng, Carlos Ramírez-Palacios, Nikolas Capra, Mattijs E. Hooghwinkel, Sebastian Thallmair, Henriëtte J. Rozeboom, Andy-Mark W. H. Thunnissen, Hein J. Wijma, Siewert J. Marrink, and Dick B. Janssen*

Cite This: *ACS Catal.* 2021, 11, 10733−10747

Read Online

ACCESS | Metrics & More | Article Recommendations | Supporting Information

ABSTRACT: ω-Transaminases (ω-TA) are attractive biocatalysts for the production of chiral amines from prochiral ketones *via* asymmetric synthesis. However, the substrate scope of ω-TAs is usually limited due to steric hindrance at the active site pockets. We explored a protein engineering strategy using computational design to expand the substrate scope of an (*S*)-selective ω-TA from *Pseudomonas jessenii* (*Pj*TA-R6) toward the production of bulky amines. *Pj*TA-R6 is attractive for use in applied biocatalysis due to its thermostability, tolerance to organic solvents, and acceptance of high concentrations of isopropylamine as amino donor. *Pj*TA-R6 showed no detectable activity for the synthesis of six bicyclic or bulky amines targeted in this study. Six small libraries composed of 7−18 variants each were separately designed *via* computational methods and tested in the laboratory for ketone to amine conversion. In each library, the vast majority of the variants displayed the desired activity, and of the 40 different designs, 38 produced the target amine in good yield with >99% enantiomeric excess. This shows that the substrate scope and enantioselectivity of *Pj*TA mutants could be predicted *in silico* with high accuracy. The single mutant W58G showed the best performance in the synthesis of five structurally similar bulky amines containing the indan and tetralin moieties. The best variant for the other bulky amine, 1-phenylbutylamine, was the triple mutant W58M + F86L + R417L, indicating that Trp58 is a key residue in the large binding pocket for *Pj*TA-R6 redesign. Crystal structures of the two best variants confirmed the computationally predicted structures. The results show that computational design can be an efficient approach to rapidly expand the substrate scope of ω-TAs to produce enantiopure bulky amines.

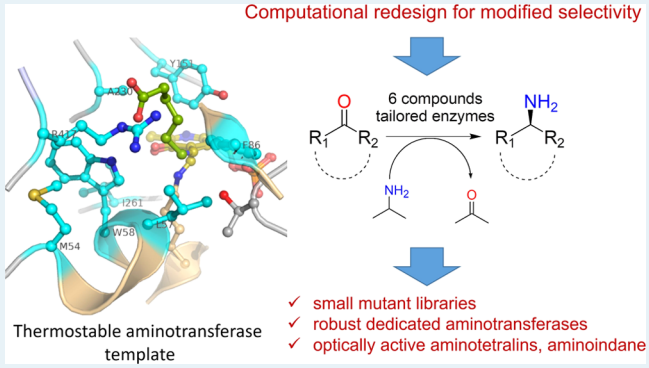

KEYWORDS: *aminotransferase, substrate scope engineering, steric hindrance, green chemistry, computer-aided design, biocatalysis, protein engineering*

INTRODUCTION

Transaminases are attractive biocatalysts for the synthesis of chiral amines, which are used as building blocks in the pharmaceutical industry.[1] In the transamination reaction, an amino group is transferred from a donor (usually an amine or amino acid) to an acceptor (a ketone, keto acid, or aldehyde) with the enzyme acting as a molecular shuttle through its cofactor, the pyridoxal 5′-phosphate (PLP) group.[2] The transaminases are very diverse, both in terms of the fold type and substrate range. The term ω-transaminase (ω-TA) is used for enzymes acting on aminoalkanoic acids with the amino and carboxylate groups on the opposite ends of an alkyl group. Most of the ω-TAs also act as general amine transaminases and do not require a carboxylate group in the amino donor or acceptor. Accordingly, such enzymes can be used to convert ketones to the corresponding amines, which is of synthetic importance if the products are enantiopure.[3]

The overall catalytic cycle of transaminases consists of two half-reactions, each composed of several reversible steps (Scheme 1).[4] In the first half-reaction, the conserved lysine that forms a Schiff base with the PLP in the native protein (internal aldimine, E-PLP) is displaced by the amino donor, resulting in the formation of an external aldimine. Then, *via* formation of quinonoid and ketimine intermediates and imine hydrolysis, the amino group is transferred to PLP, forming the aminated cofactor pyridoxamine 5′-phosphate (PMP)−

Received: May 6, 2021
Revised: July 26, 2021
Published: August 13, 2021

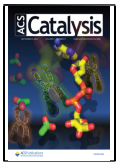

ACS Publications

© 2021 The Authors. Published by American Chemical Society

Scheme 1. Reaction Mechanism for the Transamination of Acetophenone to Enantiopure 1-Phenylethylamine with Isopropylamine as an Amino Donor[a]

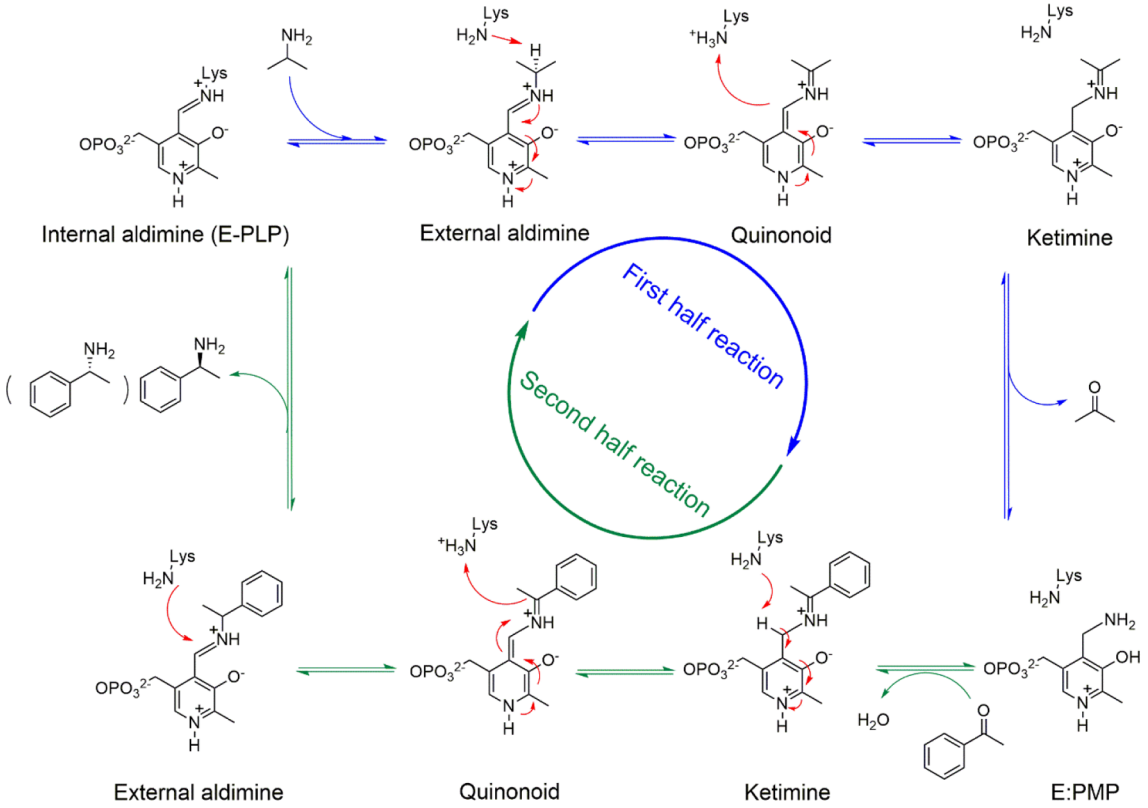

[a]Blue arrows indicate the first half-reaction, and green arrows indicate the second half-reaction. Computational efforts were aimed at redesigning the binding pocket to accommodate different external aldimine intermediates.

enzyme complex (E:PMP). The deaminated donor is released as a ketone, aldehyde, or keto acid. For the second half-reaction, the E:PMP enzyme binds the amino acceptor to regenerate the E-PLP *via* ketimine, quinonoid, and external aldimine intermediates, after which the product is released as an amine or amino acid. In the case of non-symmetric ketones, ω-TAs convert the substrate to a chiral amine, offering an attractive catalytic route for the asymmetric synthesis of chiral amines.

As with most enzymes, the substrate scope of ω-TAs is rather restricted, often due to steric hindrance in the active site.[5] Most ω-TAs are homodimeric fold-type I PLP proteins, with two identical active sites located at the interface of the monomers. Each active site of these class III transaminases has both a large and small binding pocket to accommodate substituents of the carbonyl (or amino-bound) central carbon atom.[5] While the small binding pocket can seldom accommodate anything larger than a methyl group, the large binding pocket is generally capable of accepting an aryl or alkyl group. To expand the substrate range of ω-TAs, the binding pockets need to be engineered to accept larger groups. The main strategies for finding enzyme variants capable of a desired conversion are directed evolution, rational redesign based on structure analysis, and computational redesign.[6] Several examples of engineering the selectivity of ω-TAs by directed evolution have been reported.[7−9] A prominent case is the stepwise evolution of the (*R*)-selective ω-TA (a tetrameric PLP fold-type IV enzyme) from *Arthrobacter sp.* to obtain a variant that can be used for the synthesis of the anti-diabetic drug sitagliptin from prositagliptin ketone.[8] Steric constraints in the small binding pocket and potentially undesired interactions in the large binding pocket prevent the prositagliptin ketone from being accepted by the wild-type enzyme. An enzyme variant with 27 mutations suitable for sitagliptin production was obtained after 11 rounds of stepwise evolution. Such a directed evolution campaign requires a considerable screening effort and multiple iterations of mutagenesis, sequencing, and testing.

Examination of crystal structures or homology models of ω-TAs can be used to identify target sites for mutagenesis and reduce the amount of screening required for finding desired variants.[10] This approach of rational design based on structural analysis was employed to redesign an ω-TA from *Chromobacterium violaceum* (*Cv*TA) (PDB 4A6T) to obtain derivatives that are more suitable for the kinetic resolution of 1,2-diphenylethylamine.[11] The active site architecture was investigated, and two positions in the small binding pocket were identified as potential targets for mutagenesis. A double mutant with 30-fold higher activity than the wild-type enzyme was identified. Another case is the redesign of an (*S*)-selective ω-TA from *Ruegeria sp.* TM1040 (PDB 3FCR) to produce different bulky amines.[12,13] After mutagenesis of residues around the active site, the best variants exhibited improved conversion while maintaining excellent enantioselectivity. An ω-TA from *Vibrio fluvialis* (*Vf*TA) was engineered for the synthesis of bulky amines by analysis of the X-ray structure (PDB 4E3Q) combined with structure-based bioinformatic analysis.[14] Seven residues in the active site were targeted, and

https://doi.org/10.1021/acscatal.1c02053
ACS Catal. 2021, 11, 10733−10747

Scheme 2. Synthesis of Chiral Amines (1b−6b) from Ketones (1a−6a) by *Pj*TA-R6 Mutants under the Employed Reaction Conditions

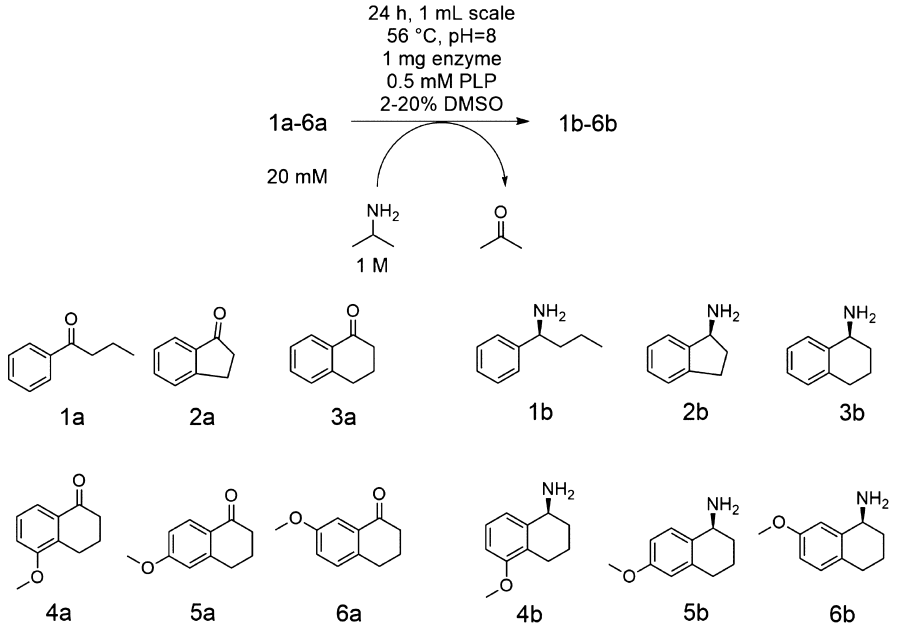

variants with high conversion and high enantioselectivity toward four amines were found.[15]

The use of computational techniques in protein engineering is becoming an attractive option, in part due to the development of better energy functions and search algorithms.[16] The caveat of using computational design is that the methodology is case-specific, and the choice of a good strategy is dependent on the enzyme family, the type of reaction, the type of substrate, and the limiting catalytic step. For ω-TAs, computational methods for finding mutations that modify the substrate scope typically include docking of a modeled reaction intermediate[17] and molecular dynamics simulations[17] or quantum mechanical modeling[18] of such an intermediate. Docking is the fastest amongst these methods, but explicit water molecules are generally not included to avoid a drastic increase in the search space. Water may play an important role in both the catalytic mechanism and shaping the binding site of ω-TAs.[18,19] Different reaction steps have been computationally modeled for the redesign of ω-TAs; hence, different ligands, that is, the ketone that acts as an amine acceptor,[17,20,21] the amine product,[22,23] the quinonoid intermediate,[12] and the external aldimine intermediate[24] have been examined. An advantage of using a reaction intermediate is that the search space for the conformation of the ligand is smaller since the positions of the PLP cofactor atoms can be considered fixed. However, working directly on a reaction intermediate implicitly assumes that the enzyme is capable of forming the Michaelis complex with the substrate (ketone or amine) and converting it to that intermediate and thus would neglect mutations that influence the entry of the substrates or their accommodation in a reactive orientation.

In computational predictions based on structural modeling, docking, and molecular dynamics simulations, mutations are usually chosen manually and investigated on a one-by-one basis, which seriously limits the accessible sequence space and complicates the prediction of variants with multiple substitutions. Alternatively, mutations can be generated in a single dock-and-design step from a user-defined search space. This way of discovering new enzyme variants without preselecting individual mutations is offered by design algorithms,[25] as implemented in, for example, Rosetta enzyme design software.[26] Often used for *de novo* protein and enzyme design, Rosetta can also be employed to modify the activity of existing enzymes.[27,28] Rosetta uses a Monte Carlo search algorithm that randomly mutates selected positions and searches for low-energy solutions by varying residue identities, protein residue rotamers, and ligand conformations.[29] Calculations are very fast, and the search space can be defined in terms of target positions, allowed mutations, and rotamer library density of target residues and ligands. Local backbone changes are allowed, and good numbers of primary designs carrying multiple mutations can be generated in a single dock-and-design step. The CASCO protocol employs Rosetta in combination with MD simulations for ranking.[30] In the current work, we present a design strategy that uses Rosetta and employs the Rosetta interface energy as the main metric for the ranking of primary design mutants, obviating the need for more expensive MD simulations in the initial ranking phase. The strategy benefits from the target ligands having hydrophobic and rigid substituents;[31] hydrophobic groups do not form hydrogen bonding networks involving water molecules, which are typically absent in docking approaches. Furthermore, we use docking with the target substrates covalently bound to the PLP in the form of the external aldimine intermediate, which greatly reduces the degrees of freedom of the binding poses and thereby the search space.

As the target enzyme, we have chosen a recently reported stabilized variant of the (*S*)-selective ω-TA from *Pseudomonas jessenii* (*Pj*TA-R6, T_m^{app} 85 °C).[32] The enzyme was engineered for increased stability by computational redesign of the subunit interface and catalyzed enantioselective production of (*S*)-1-phenylethylamine at high substrate concentration [100 mM acetophenone, 1 M isopropylamine (IPA)] and in the presence of 20% dimethyl sulfoxide (DMSO) at 56 °C. In view of the excellent performance of *Pj*TA-R6 under these harsh reaction conditions, we considered *Pj*TA-R6 to be a good template

https://doi.org/10.1021/acscatal.1c02053
ACS Catal. 2021, 11, 10733−10747

enzyme to broaden the catalytic scope toward the production of enantiopure bulky and cyclic primary amines. As target products, we chose six different bulky (*S*)-amines (Scheme 2), with structures that are quite different from the accepted substrate (*S*)-1-phenylethylamine. First, (*S*)-1-phenylbutylamine (**1b**) was chosen in view of the bulkiness of the propyl group that should be accommodated in the small binding pocket of *Pj*TA-R6. Moreover, (*S*)-1-phenylbutylamine has been the target of previous transaminase engineering efforts.[12,17,21,22,33] Two other target amines were (*S*)-(+)-1-aminoindan (**2b**) and (*S*)-(+)-1-aminotetralin (**3b**). The activity of *Pj*TA-R6 for these compounds is undetectable; the same is observed with most other ω-TAs.[22,23,34−36] The last three selected bulky amines [(*S*)-5-methoxytetralin-1-amine (**4b**), (*S*)-6-methoxytetralin-1-amine (**5b**), and (*S*)-7-methoxytetralin-1-amine (**6b**)] have not yet been synthesized by ω-TAs and possess an even more bulky group than **3b** to be accommodated in the large binding pocket. The corresponding ketones used as substrates are butyrophenone (**1a**), 1-indanone (**2a**), 1-tetralone (**3a**), 5-methoxy-1-tetralone (**4a**), 6-methoxy-1-tetralone (**5a**), and 7-methoxy-1-tetralone (**6a**) (Scheme 2).

The employed strategy aims to produce, in a single Rosetta dock-and-design step, enzyme variants with mutations that facilitate the accommodation of the external aldimine intermediate of the target reactions. The search space included multiple residues around the active site (Table S1), and the resulting small mutant libraries selected for experimental verification contained mutations at eight positions of *Pj*TA-R6 (Scheme 3). The ability of the Rosetta-generated variants to accommodate the intended intermediates was evaluated by the Rosetta interface energy (docking score).[37] The results showed that there is a correlation between the interface energy and the experimental yield, which can aid in narrowing down the search in future mutagenesis efforts. Experimental verification showed that the majority (97%) of the mutants gave better reactivity than the initial scaffold, which was not able to produce any of the six targeted amines. All mutants showed excellent enantioselectivity for the production of the (*S*)-amine.

Scheme 3. Schematic View of the Large and Small Binding Pockets of *Pj*TA-R6 Bearing the External Aldimine Intermediate [PLP-Schiff Base with (*S*)-1-Phenylethylamine][a]

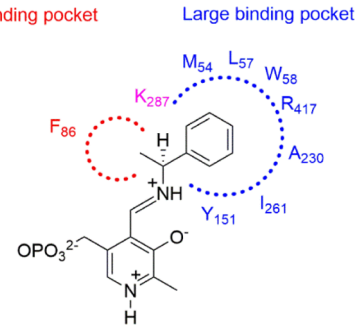

[a]Target residues belonging to the large binding pocket are colored blue, and the target residue from the small binding pocket is colored red. K287 is the catalytic lysine

MATERIALS AND METHODS

Computational Library Design. The crystal structure of *Pj*TA-R6 (PDB 6TB1) served as a scaffold for docking of the target ligands. The scaffold was prepared by explicitly adding hydrogen atoms to the crystal structure of *Pj*TA-R6 using an automatic Yasara procedure (the CleanAll and OptHydAll functions).[38] All crystallized water molecules and ions were deleted from the structure. The modeled ligands are the external aldimines of **1a−6a**, named, respectively, as **1EA−6EA** in this manuscript (Figure S1). Structures of **1EA−6EA** were prepared by adding a covalent bond between the PLP C4′ atom and the corresponding amino substrate (**1b−6b**) to form the respective Schiff base. Geometry optimization of the resulting external aldimine structures was performed with the semiempirical AM1 method using the COSMO implicit solvent model.[39] Partial charges were derived using the AM1/BCC procedure.[40] Rotamer libraries for ligands **1EA** and **4EA−6EA** were generated by random perturbation of non-hydrogen atom dihedrals (SampleDih Yasara routine) (Figure S1). Atoms originally belonging to the pyridoxal cofactor were kept fixed. Ligands **2EA** and **3EA** were represented by a single rotamer. The ligands (**1EA−6EA**) were initially aligned to the cofactor atoms originally found in the crystal structure. This initial conformation along with the rotamer library served as input for Rosetta design to generate the enzyme complexes containing the external aldimine ligands.[26] For this computational design, we used Rosetta build number 57,849, and for comparing experimental activities with interface energies, we used Rosetta build number 60,072, which outputs energies in kcal/mol. The following command line arguments were used for Rosetta docking: -enzdes, -cst_predock, -cst_design, -cut1 0.0 -cut2 0.0, -cut3 8.0, -cut4 10.0, -cst_min, -chi_min, -bb_min, -packing:use_input_sc, -packing:soft_rep_design, -design_min_cycles 3, -ex1:level 4, -ex2:level 4, -ex1aro:level 4, and -ex2aro:level 4. All residues within 10 Å of any ligand non-hydrogen atom were set to repackable, but residues 152, 225, 258, 119, 118, 324, 292, 59, 287, and 87 were set to NATRO (NATural ROtamer). Multiple runs were performed for each substrate, and varying combinations of residues were allowed to mutate (Table S1). For each run, 1000 decoys were generated, and the resulting mutants were ranked by their Rosetta interface energy. Figures representing Rosetta designs were created with VMD (https://www.ks.uiuc.edu/Research/vmd/).

In general, ranking mutants by the interface energy of the external aldimine complex proved to be a good target function to guide mutagenesis (see the Results section). However, as an extra step to explain some outliers, the water displacement that would accompany substrate binding was estimated using MD simulations. These simulations were performed with enzyme−cofactor and enzyme−ligand complexes generated by Rosetta docking using GROMACS 2020 software and the AMBER99SB force field. Details are given in the Supporting Information.

Mutagenesis, Enzyme Expression, and Purification. Mutations were introduced in vector pET-20b (+)-His-*Pj*TA-R6[32] *via* QuikChange mutagenesis and confirmed by DNA sequencing (Eurofins Genomics). *Pj*TA variants were produced in *Escherichia coli* BL21(DE3) cultivated in 200 mL of Terrific Broth (TB) medium with 100 μg/mL ampicillin. Expression was induced with IPTG at OD_{600} 0.6,

https://doi.org/10.1021/acscatal.1c02053
ACS Catal. 2021, 11, 10733−10747

and cultivation was continued at 24 °C for 16 h. Cells were harvested by centrifugation, washed, and lysed by sonication in 20 mM potassium phosphate, pH 7.5, containing 500 mM NaCl and 20 μM PLP. Centrifugation (36,000×*g*, 45 min, 4 °C) gave cell-free extract, loaded on a 5 mL HisTrap column. Elution with a linear gradient of 0−500 mM imidazole in 20 mM potassium phosphate, pH 7.5, containing 500 mM NaCl and 20 μM PLP, followed by desalting with Econo-Pac 10DG columns (Bio-Rad) gave purified enzymes. Protein concentrations were determined with the Bradford assay, and purified enzymes were stored in aliquots at −80 °C in 50 mM potassium phosphate, pH 8.0, with 20 μM PLP.

Thermal Shift Assays. Apparent melting temperatures (T_m^{app}) were measured by a fluorescence-based thermal shift assay (Thermofluor).[41] Specifically, in the wells of an IQ 96-well PCR plate (Bio-Rad), enzyme samples of 20 μL (0.5 mg/mL protein in 50 mM potassium phosphate buffer, pH 8.0) were mixed with 5 μL of 50-fold diluted SYPRO Orange. The plates were sealed with the Microseal B adhesive sealer (Bio-Rad) and heated from 20 to 99 °C in a MyiQ real-time PCR machine (Bio-Rad) at a heating rate of 1 °C/min. The temperature at which the rate of fluorescence change (-dRFU/dT) was highest was taken as T_m^{app}.[42] For determining stability under harsh conditions, enzyme samples for thermal shift assays were prepared in 50 mM phosphate buffer containing 1 M IPA, 20% DMSO, or both of these. The pH was set at 8.0.

Reagents. IPA, ketones (**1a**−**6a**), (*S*)-amines (**1b**−**6b**), and (*R*)-amines (**1c**−**6c**) (except **4b** and **4c** due to unavailability) (Figure S2) were purchased from Sigma-Aldrich. Synthesis of compounds **4b** and **4c** was attempted by redesigned *Pj*TA-R6 variants; only a single enantiomer was obtained, and its identity was confirmed by gas chromatography mass spectrometry (GC−MS). PLP was purchased from Fisher Scientific. The purity of reagents was higher than 95%.

Enzyme Reactions. Transaminase-catalyzed amination reactions were performed at 1 mL scale in sealed glass vials at 56 °C using 50 mM potassium phosphate buffer, pH 8.0, containing 1 M IPA, 20 mM one of the ketones **1a**−**6a**, 20% DMSO (or 2% DMSO in the case of **2a** and 15% in the case of **3a**), 0.5 mM PLP, and 1 mg of purified enzyme. For analysis, 100 μL samples were quenched by adding 20 μL of 10 M NaOH, centrifuged, and extracted twice with 300 μL of ethyl acetate. The combined extracts were treated with anhydrous magnesium sulfate to remove water, and a total of 200 μL of each sample was used for GC analysis. Because of the instability of amines **4b**, **5b**, and **6b**, they were derivatized to the acetamide before GC analysis.[35] For this, 200 μL samples of the extracted products were mixed with 300 μL of acetic anhydride and 5 mg of 4-dimethylaminopyridine (DMAP). After 1 h reaction time (450 rpm, room temperature), samples were treated with 500 μL of water, and the organic layers were dried with anhydrous magnesium sulfate. The dried samples were used for GC analysis.

Kinetic parameters of transaminase reactions were determined by measuring depletion of aromatic ketones in the 96-well microplate format. The reaction mixtures (1 mL) contained 1 M IPA, varying concentrations (0−16 mM) of ketones (**1a**−**6a**), 0.05 mM PLP, and 0.05 mg/mL purified enzyme in 50 mM potassium phosphate buffer, pH 8.0. Reactions were performed at 56 °C and started by addition of the enzyme. At different times (1 min, 2 min, 4 min, and 8 min), 200 μL samples were quenched by adding 50 μL of 0.2 M NaOH. After centrifugation, 200 μL samples were transferred to a 96-well microplate, and the absorbance was measured in a plate reader. Samples from reaction mixtures with 2−16 mM ketone were diluted 2−16-fold before measurement. The depletion of ketones **1a**, **2a**, and **3a**−**6a** was detected at 290, 310, and 320 nm, respectively, and initial rates were calculated using calibration curves (0−1 mM).

GC Analysis. The concentration and enantiopurity of amines **1b**−**6b** were determined by chiral GC. Calibration was done with mixtures of racemic amines and the corresponding ketones (0.2, 2, and 20 mM) dissolved in the standard reaction system but without addition of the enzyme. Peaks for ketone, (*S*)-amine, and (*R*)-amine were identified with commercial standards. Because of the structural similarity to **5b** and **6b**, **4b** was quantified using the same GC response curve. For details, see Supporting Information Figures S3−S9.

Crystal Structures. Before crystallization, *Pj*TA variants W58G and W58M + F86L + R417L were further purified using a Superdex 200 13/300 column (GE Healthcare), equilibrated with 20 mM HEPES, pH 7.5, 100 mM NaCl, and 20 μM PLP. Proteins were concentrated to ∼8 mg/mL using a Vivaspin Turbo 4 10K filter unit (Sartorius) and crystallized using hanging drop vapor diffusion in 24-well LINBRO plates (Molecular Dimensions Ltd). Per well, 1 μL of protein solution was mixed with 1 μL of reservoir solution containing 0.7−1.0 M sodium succinate, pH 7.6, as in our previous work on the thermostable parent *Pj*TA-R6.[32] Crystals of *Pj*TA-R6 + W58G appeared after two days and grew to an average size of 0.4 × 0.3 × 0.3 mm^3. Their yellow color indicated that PLP was bound. Large yellow crystals were also obtained for *Pj*TA-R6 + W58M + F86L + R417L, with an average size of 0.3 × 0.3 × 0.2 mm^3. Attempts to obtain structural information on the binding mode of the external aldimine included several soaking experiments with the amino donor IPA, the ketones **1a** and **2a**, or the amines **1b** and **2b** for variants *Pj*TA-R6 + W58M + F86L + R417L and *Pj*TA-R6 + W58G. X-ray diffraction data were collected at beamlines I24 and I04 at Diamond Light Source (Oxford, UK). The diffraction data were indexed and integrated using xia2/Dials[43] and then scaled and merged with Aimless[44] from the CCP4 software suite.[45] The crystals of *Pj*TA-R6 + W58G and *Pj*TA-R6 + W58M + F86L + R417L belonged to the same space group as *Pj*TA-R6, with nearly identical unit cell dimensions, allowing the *Pj*TA-R6 structure (PDB 6TB1) to be used for initial refinement and electron density map calculations. Subsequently, the structures were adjusted by model building to replace the side chains of the mutated residues. After a few cycles of refinement with RefMac5[46] followed by model building and water placement with Coot,[47] the structure was completed. A summary of data collection is provided in Table S3. Figures showing crystal structures were produced with PyMOL.[48]

RESULTS

Computational Design of *Pj*TA Variants. To examine the use of a single dock-and-design step for shifting the substrate range of a transaminase toward acceptance of more bulky substrates, we selected the *Pj*TA-R6 variant of the transaminase from *P. jessenii* as the template. *Pj*TA-R6 is a thermostable variant (T_m^{app} = 85 °C) of the native 6-aminohexanoate transaminase (*Pj*TA, T_m^{app} = 62 °C) of the caprolactam biodegradation pathway. *Pj*TA-R6 contains six point mutations (P9A + E38Q + A60V + S87N + M128F + I154V) that increase its thermostability, of which positions 60, 87, and 154 are located near the active site. It does not accept

https://doi.org/10.1021/acscatal.1c02053
ACS Catal. 2021, 11, 10733−10747

Table 1. Mutant Dataset for the Asymmetric Synthesis of 1b−6b

mutant	no.	target amines	Rosetta interface energy (kcal/mol)	ΔT_m^{app} (°C)[a]	yield (%)	ee (%)
*Pj*TA-R6[b]	1	**1b−6b**	-[c]	0	n.a.[d]	n.m.[e]
W58G[f]	2	**2b−6b**	−21.6/−22.3/−22.3/−22.8/−21.5	0	51/64/86/29/69	>99
W58G + F86S	3	**1b**, **3b**, **4b**	−21.8/−22/−21.7	−8	52/30/47	>99
W58G + F86L	4	**3b**	−21.9	+2	27	>99
F86L + Y151F	5	**1b**	−23	−11	38	>99
L57D + Y151F	6	**2b**	−21.6	+1	n.a.	n.m.
W58G + F86L + R417L	7	**1b−4b**, **6b**	−21.7/−21.4/−22.3/−21.3/−21.6	+3	49/12/43/72/16	>99
W58M + F86L + R417L[f]	8	**1b**	−22.9	−5	72	>99
W58G + F86S + A230G	9	**1b**	−21.1	−1	2	>99
W58G + F86S + R417L	10	**1b**, **2b**, **3b**	−21.9/−21.3/−22.4	+4.5	31/6/27	>99
W58G + F86S + I261A	11	**1b**, **4b**	−21.2/−20.6	−8	11/8	>99
W58G + F86N + R417L	12	**2b−6b**	−21.3/−22.4/−20.8/−19.9/−21.7	−2	7/33/62/12/32	>99
W58G + F86N + R417F	13	**3b−6b**	−22.4/−21.4/−20.2/−21.7	−3	33/59/12/28	>99
W58G + F86L + R417F	14	**3b−6b**	−22.3/−21.2/−20.5/−21.6	−6.5	44/70/17/20	>99
W58G + F86N + R417I	15	**4b**	−21	−5	66	>99
W58G + F86L + R417I	16	**4b**	−20.8	−3	69	>99
M54T + W58G + R417L	17	**4b**	−21.6	+2	78	>99
M54T + W58G + R417I	18	**4b**	−21.7	+2	57	>99
M54T + W58G + R417Q[g]	19	**4b**	−21	−34	1	>99
M54T + W58G + F86S	20	**5b**	−22.7	−8	1	>99
M54T + W58G + F86L	21	**5b**	−22.4	−3	2	>99
W58G + F86L + I261N	22	**5b**	−20.7	−11	1	>99
W58G + F86C + A230P + R417L	23	**1b**	−21.6	0	37	>99
W58G + F86S + A230G + R417L	24	**1b**	−21.5	−1	37	>99
W58G + F86N + A230G + R417L	25	**1b**	−21.5	−5.5	28	>99
L57E + W58G + Y151F + R417K	26	**2b**	−21	−3.5	n.a.	n.m.
W58G + F86L + I261A + R417L	27	**1b**, **2b**	−21.2/−20.7	−7	21/1	>99
W58G + F86L + I261V + R417L	28	**3b**	−22.1	−4	37	>99
W58G + F86L + I261V + R417F	29	**3b**	−22.1	+1	39	>99
W58G + F86L + I261A + R417F	30	**3b**	−21.5	+5.5	14	>99
W58G + F86S + I261A + R417L	31	**3b**	−21.6	+6	9	>99
M54T + W58G + F86S + R417L[g]	32	**4b**	−20.8	−32	15	>99
M54T + W58G + F86L + R417I[g]	33	**4b**	−21	−33	14	>99
W58G + F86L + A230P + I261V	34	**5b**, **6b**	−20.8/−19.1	−5	5/4	>99
M54T + W58G + I261A + R417L	35	**5b**	−18.4	−1	1	>99
W58G + F86L + A230P + I261V + R417L	36	**4b**, **6b**	−20/−19.9	−5	20/12	>99
W58G + F86N + A230P + I261V + R417L	37	**4b**, **6b**	−19.9/−20	−2	6/7	>99
W58G + F86L + A230P + I261V + R417I	38	**4b**, **5b**, **6b**	−19.2/−19.3/−19.6	−2	14/4/4	>99
W58G + F86L + A230P + I261V + R417Q	39	**6b**	−21.1	0	11	>99
M54T + W58G + F86L + A230P + I261V + R417L	40	**4b**, **6b**	−19.5/−19.1	−2	9/4	>99
M54S + W58G + F86L + A230P + I261V + R417L	41	**6b**	−19.1	−3	5	>99

[a]The difference in T_m^{app} between *Pj*TA-R6 and mutants. [b]T_m^{app} of *Pj*TA-R6 is 85 °C. [c]Interface energies were not determined since no catalytic poses were obtained. [d]n.a. = no activity. [e]n.m. = not measured. [f]The mutant with the best analytic yield of the corresponding amine. [g]Variants with poor stabilities.

any of the ketones **1a−6a** as substrates for transamination to **1b−6b**, respectively.

Derivatives with an expanded substrate acceptance were predicted using Rosetta in a single dock-and-design step.[49] Rosetta design calculations were performed for each of the substrates **1a−6a** by optimizing the active site for binding of the corresponding external aldimine intermediates **1EA−6EA** (Figure S1). Reshaping the binding pocket of *Pj*TA-R6 was mainly aimed at alleviating steric hindrance caused by the bulky hydrophobic substituent on the carbonyl carbon of the substrate. Based on structural inspection of the crystallographic structure of the external aldimine formed from 6-amino-hexanoic acid by *Pj*TA (PDB 6G4E), the search space comprised residues near the binding site (Table S1).

For each ligand, 3−5 independent dock-and-design runs were performed, and in each run, 4−6 active site residues were allowed to mutate. The number of runs and the identity of the residues selected for mutagenesis were case-specific for each compound (Table S1).

The runs generated approximately 100−400 unique primary designs per ligand. These designs were ranked on the basis of their Rosetta interface energy, and the top 10−20 enzyme variants were selected. The resulting designed libraries contained mutations on positions Met54, Leu57, Trp58, Tyr151, Ala230, Ile261, and Arg417, belonging to the large binding pocket, and on position Phe86, belonging to the small binding pocket. Finally, 7−18 of the top-scoring mutants for each substrate were selected for experimental verification (Table 1). No enzyme variant was manually added to the

https://doi.org/10.1021/acscatal.1c02053
ACS Catal. 2021, 11, 10733−10747

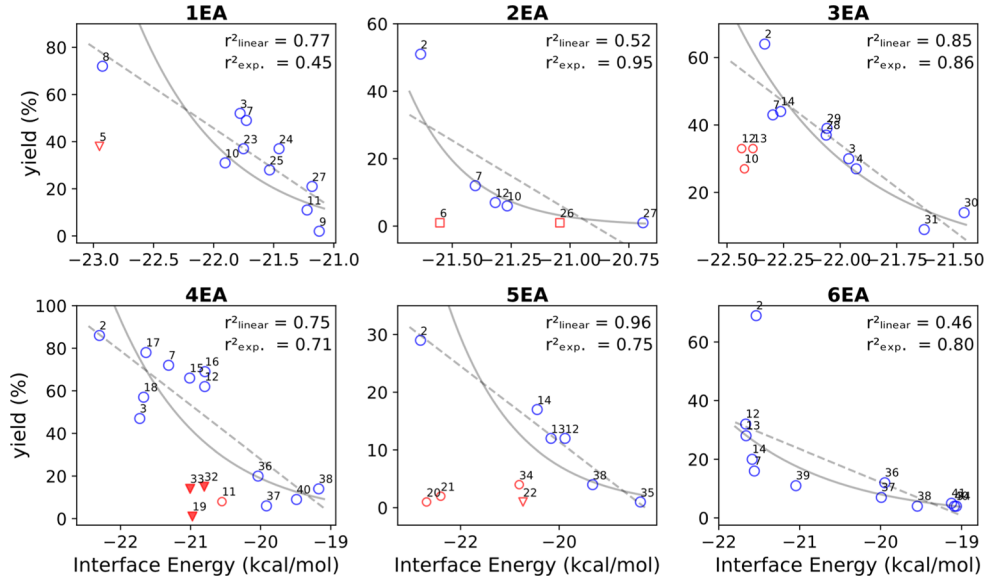

Figure 1. Comparison of the Rosetta interface energies and the experimental analytical yields of *Pj*TA-R6 variants redesigned for the asymmetric synthesis of six amines. In most cases, the best mutant is correctly identified by the docking score. Outliers (*i.e.*, variants not following the overall trend) are colored red. Some outliers have a large (filled triangles, mut19, mut32, and mut33) or minor (open triangles) reduction of T_m^{app}. Others have a structure not suitable for catalysis (red squares), and the rest of outliers are in red circles. Dotted lines are linear regression (r_{linear}^2), and continuous lines are semilog regression (r_{exp}^2). Non-outliers (blue circles) were used for regression. Further information about the criteria used to define or classify outliers is given in the Supporting Information.

dataset. In total, 70 Rosetta designs were selected, which included 40 designs with different sequences because some designs for different substrates had the same sequence.

Experimental Verification of Amine Synthesis. All 40 unique designed mutants were constructed by site-directed mutagenesis. They expressed well in the soluble form in *E. coli* and were purified (Table 1). All but two of the mutant enzymes showed the desired catalytic activity and displayed high enantioselectivity (ee > 99%) for the production of chiral amines **1b**−**6b**. Amine yields in these asymmetric transformation reactions varied from 1−86%, the latter value being similar to what was obtained with *Pj*TA-R6 in the synthesis of (*S*)-1-phenylethylamine from its preferred substrate acetophenone. Reactions were done with 1 M IPA in the presence of 20% DMSO, indicating that the robustness that was engineered previously into *Pj*TA-R6 was well maintained.

Gratifyingly, there was reasonable agreement between the docking results and yields in amine synthesis (Figure 1). In general, better Rosetta interface energies of the external aldimines **1EA**−**6EA** correlated with higher yields in amination reactions. The best variant for the synthesis of amines **1b**−**6b** either was the top-ranking variant (for compounds **2**, **4**, and **5**) or occurred among the top-ranking variants (compounds **1**, **3**, and **6**) based on the interface energy (Table 1). This indicates that the computed Rosetta interface energies can be helpful to distinguish the best-performing variants among the larger numbers of primary designs generated using the Rosetta search algorithm.

The trend between these docking scores and experimental yields was not followed by all redesigned *Pj*TA-R6 derivatives. A possible cause could be that underperforming variants are less stable and inactivated under the harsh conditions of the amination reactions (56 °C, 1 M IPA, 2−20% DMSO). Since the selection of designs for experimental verification was based on scoring of Rosetta interface energies and did not consider possible effects of mutations on stability, we examined the thermostability of all the designed *Pj*TA-R6 variants (Table 1). Only 3 out of 40 variants had substantially lower thermostability than *Pj*TA-R6 (mutants 19, 32, and 33; ΔT_m^{app} from −34 to −32 °C). Of the other 37 designs, 22 had a modest reduction of thermostability (ΔT_m^{app} from −2 to −11 °C), whereas 12 variants showed the same or slight increase in stability.

The loss of thermostability of variants 19, 32, and 33 was indeed accompanied by a detrimental effect on the yield of amine **4b** under the harsh conditions of the reactions (56 °C, 1M IPA, 2−20% DMSO) in comparison to variants that were designed for the same product and showed higher stability (variants 15−18) (Table 1). Nevertheless, the three unstable variants still gave a higher yield of amine **4b** than the parent *Pj*TA-R6 enzyme, which may be due to some initial activity, followed by inactivation under turnover conditions. Mutant 20 (ΔT_m^{app} = −8 °C) also was less thermostable than the parent and gave a lower yield than expected from the trends shown in Figure 1 (**5EA**).

To further examine the role of enzyme stability under reaction conditions, three variants with different thermostabilities were used to test the effect of DMSO and/or IPA in thermal shift assays, (i.e., variant 8, variant 19, and variant 20) (Table S2). Variant 8 (T_m^{app} = 80 °C), which followed the trend between yield and Rosetta interface energy (Figure 1, **4EA**), had normal stability in the presence of DMSO or IPA. It was partially inactivated and showed reduced stability only after prolonged incubation under reaction conditions. The less-thermostable variant 19 (T_m^{app} = 51 °C) was partially unfolded and very sensitive to a high concentration of IPA or DMSO, as indicated by a further reduction of T_m^{app} (Table S2). Initial ketone conversion activities in the presence of IPA and DMSO were also determined, using a ketone concentration of 20 mM. According to the Rosetta interface energies, variant 19 was expected to be about half as active as variant 2, but its activity with ketone **4a** in the presence of DMSO and IPA (0.06 U/

https://doi.org/10.1021/acscatal.1c02053
ACS Catal. 2021, 11, 10733−10747

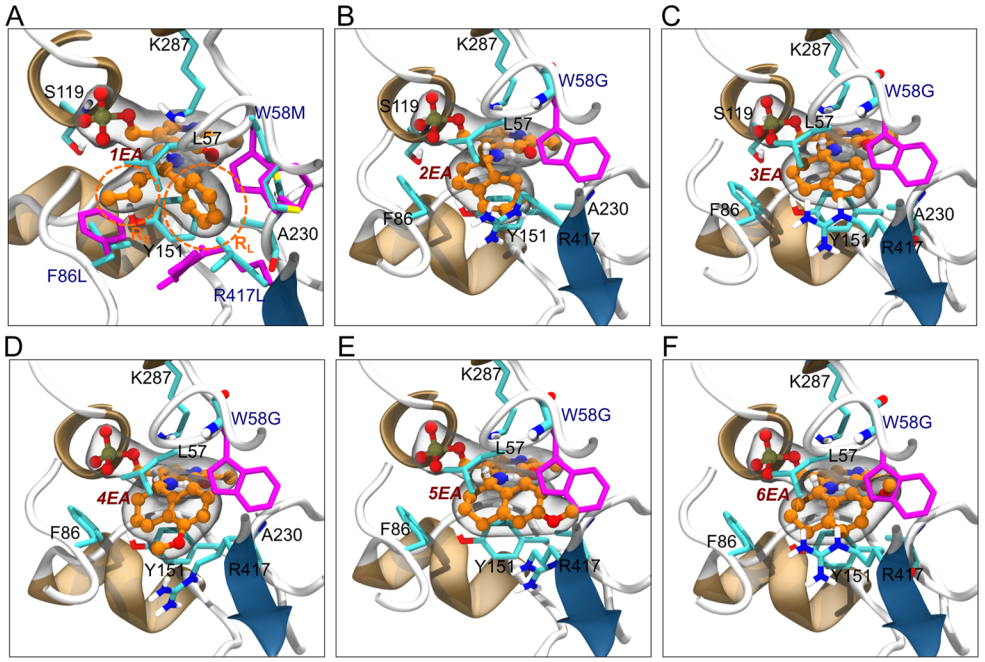

Figure 2. Designed binding sites for external aldimines. (A–F) Rosetta-docked external aldimine complexes (orange) of enzyme variants *Pj*TA-R6 + W58M + F86L + R417L for **1EA** (A) and *Pj*TA-R6 + W58G for **2EA–6EA** (B–F). Amino acids of designed variants are colored in cyan (carbon), red (oxygen), and blue (nitrogen). Non-polar hydrogens are not shown, with the exception of hydrogen H_α, that is, the hydrogen abstracted from the external aldimine (Figure S12). The superimposed crystal structure with the non-substituted residues of *Pj*TA-R6 (magenta) is shown for comparison [*i.e.,* Trp58, Arg417, and Phe86 in panel (A) and Trp58 in panels (B–F)]. Figures were rendered using VMD.

mg) was more than 10-fold lower than with variant 2 (T_m^{app} = 85 °C), which had retained stability and activity under these conditions (0.7 U/mg). In the presence of 20% DMSO and 1 M IPA, the initial rate of conversion of **5a** by variant 20 (T_m^{app} = 77 °C) was rather low (0.04 U/mg), and the yield of amine was also lower than expected from the Rosetta interface energy calculated for **5EA** (Figure 1). These results indicate that the reduced stability found with some variants was detrimental for amination reactions due to the harsh reaction conditions and explains some of the outliers in Figure 1. Besides loss of stability, a possible cause of deviations from the relationship between interface energy and performance in synthesis is the occurrence of a structure unsuitable for catalysis (see below).

Causes and Effects of Reduced Thermostabilities. A closer inspection of mutants 32 and 33 revealed that a single mutation is responsible for the drastic reduction in thermostability. While mutants M54T + W58G + R417[L/I] showed excellent yields in the production of **4b**, introducing mutation F86[S/L] substantially lowered amine production and decreased the T_m^{app} by more than 30 °C. The mutations F86[L/S] were intended to alleviate steric clashes of Phe86 with the tetralin moiety (Figure S10). The structural models showed that Phe86 has $\pi-\pi$ interactions with Tyr20 and Arg417. The latter in turn interacts with Asn87, which was previously introduced by an S87N substitution that enhances thermostability. Most other mutants carrying a substitution on position F86 showed a small reduction in thermostability [25 F86X mutants showed decreased thermostability, whereas six were more thermostable (cutoff of 1 °C)]. In variants 5 and 26, which maintained Phe86, mutation of Tyr151 led to a reduction in thermostability, which we attribute to the loss of an interaction *via* a water molecule with the phosphate of the PLP group (Figure S11).[50] Overall, we found the template *Pj*TA-R6 to be robust enough to accept the majority of the proposed mutations with no substantial decrease in T_m^{app}, but the effect of some of the mutations on the thermostability of the enzyme was difficult to predict. This especially holds for variants carrying multiple mutations that remove and create interactions that contribute to stability.

Rationalization of the Observed Activities. To examine if the observed activities of the Rosetta designs can be rationalized, we inspected the predicted structures (Figure 2). Variant *Pj*TA-R6 + W58M + F86L + R417L was the best-performing mutant for the asymmetric synthesis of **1b**, giving an amine yield of 72%. In this and other designs optimized for **1b**, mutation of Trp58 to Met turned out to be better for accommodating **1EA** than mutation W58G, which also occurred frequently (*e.g.*, *Pj*TA-R6 + W58G + F86L + R417L; 49% yield). While mutation W58G only eliminates steric hindrance, mutation W58M maintains a more hydrophobic binding site in addition to eliminating protein–ligand steric clashes (Figure S11). This should lead to better hydrophobic contacts with the propyl substituent on the carbonyl carbon of **1b**. The larger cavity produced by mutation W58G will require more water molecules to be displaced upon substrate binding than the smaller cavity left by mutation W58M and offers fewer stabilizing van der Waals interactions. In further engineering efforts of *Pj*TA-R6 aimed at improving activity with substrates where the large substituent is a phenyl group, the mutation W58M should be considered.

Ketones containing the indane (**2a**) or tetralin (**3a–6a**) group required a *Pj*TA-R6 variant with mutation W58G to function as an amino acceptor. In the external aldimine form, the aromatic ring of indane or tetralin must bind in the large binding pocket for production of the (*S*)-enantiomer of the amine. Unlike the aromatic ring in **1EA**, the indane and tetralin bicyclic structures of **2EA–6EA** allow no rotational mobility for the aromatic ring, causing steric hindrance with Trp58. The

https://doi.org/10.1021/acscatal.1c02053
ACS Catal. 2021, 11, 10733–10747

W58G single mutation was enough to alleviate this steric hindrance, and the *Pj*TA-R6 + W58G mutant produced enantiopure (*S*)-amines **2b**−**6b** in yields ranging from 29 to 86% (Table 1). Additional mutations on top of W58G also gave active variants for conversion of ketones **2a**−**6a** to amines but did not have a further beneficial effect, which was reflected in both the Rosetta interface energy and the experimental data. All variants carrying multiple mutations remained active and highly enantioselective.

From the experimentally tested mutant library of 40 unique variants (70 different enzyme−ligand combinations), only two variant−ligand combinations did not exhibit catalytic activity toward the intended compound. The L57D + Y151F (mutant 6) and L57E + W58G + Y151F + R417K (mutant 26) derivatives of *Pj*AT-R6 were inactive on **2a** (Figure 1), and neither was capable of accommodating **2EA** in a catalytic pose, as confirmed by visual inspection of the designed structure (Figure S12). In variant *Pj*TA-R6 + L57D + Y151F, the aromatic ring of the bicyclic indane group of **2EA** cannot be accommodated due to steric clashes with Trp58, which the mutations L57D + Y151F did not alleviate. Thus, no catalytic pose was obtained in the docking procedure, rendering the calculated Rosetta interface energy for this mutant irrelevant for predicting catalytic potential. Furthermore, mutation L57D introduced a hydrogen bond between the side chains of Asp57 and Thr324, which might cause the mutant to be inactive even if the steric clashes with Trp58 were to be alleviated. Residue Thr324 is believed to assist Lys287 in catalysis by forming a hydrogen bonding network.[19] Glu57 in variant *Pj*TA-R6 + L57E + W58G + Y151F + R417K can be disruptive for the very same reasons. Additionally, the formation of a salt bridge between Glu57 and Lys417 may prevent free movement of Glu57 upon substrate binding, causing steric clashes with the indane moiety, rendering the enzyme inactive (Figure S12). The steric clashes were reflected in the poor interface energy of mutant *Pj*TA-R6 + L57E + W58G + Y151F + R417K (Table 1 and Figure 1). Thus, for the two designs, we propose a combination of steric hindrance and disruption of catalytic conformations as the cause of inactivity in the production of **2b**.

The computational framework also yielded *Pj*TA-R6 mutants suitable for the production of **3b**. Due to the bicycle rigidity, the aromatic ring of the tetralin moiety has steric clashes with Trp58 of *Pj*TA-R6 (Figure 2), which were eliminated by mutation W58G. The tetralin differs from the native substrate 6-aminohexanoic acid in that the latter is flexible and points outward into the tunnel where it forms a salt bridge with Arg417, thus avoiding steric clashes with Trp58 (Figure S13). In fact, the best variant for the production of **3b** was the single mutant *Pj*TA-R6 + W58G, and additional mutations did not improve the yield. Furthermore, a design run in which Trp58 was not allowed to mutate did not result in designs with a good docking score (Table S1).

The different positions of the methoxy group attached to the tetralin moiety in intermediates **4EA**, **5EA**, and **6EA** created distinctive trends. Most of the mutants designed to accommodate **4EA** showed higher yields than designs for **5EA** or **6EA**. This difference can be rationalized by the position of the methoxy group in the tetralin moiety. The 5-methoxy substituent on the phenyl group of **4EA** points toward the binding site entrance, making it easier to fit **4EA** in the large pocket (Figures 2D and S14) than **5EA** or **6EA**. In other variants, the position of the methoxy group could act in favor of **6EA**; the mutation R417Q was found to be beneficial for accommodating **6EA**, increasing the product yield from 4% (mutant 34) to 11% (mutant 39) (Table 1). The side chain $-NH_2$ of Gln417 can form a hydrogen bond with the oxygen lone pairs of −OMet (O−H distance of 2.0 Å) in the case of **6EA**, but such a hydrogen bond would not form with **4EA** as the −OMet is too far away (>5Å) (Figure S14B). Accordingly, in the series M54T + W58G + R417X, where X = L, I, and Q, the product yields decreased from 78 to 1% (Table 1). It must be noted that the abovementioned rationalization only considers protein−ligand binding interactions of catalytic conformations of the complex but not the intrinsic ligand reactivities as the cause for differences in the observed reaction yields.

Effect of Mutations on the Hydrophobicity of the Binding Site. As mentioned above, most mutants with better Rosetta interface energy scores were better at converting ketones **1a**−**6a** to the corresponding amines, and some variants deviating from this trend had a reduced thermostability. To explain a few outliers that dot not have a decreased thermostability, that is, red circles in the **3EA**, **4EA**, or **5EA** datasets (Figure 1), we examined if the number of water molecules that would need to be displaced for the tetralin moiety to fit in the binding pocket could play a role (Figure S15). A large displacement of water molecules may significantly impact the binding energy of ligands.[51,52] We used ns-scale MD simulations to quantify the difference in the water-accessible volumes of the Rosetta-generated structures (Figure S16). Although this approach did not explain the outliers of **3EA**, **4EA**, or **5EA**, when considering all variants (outliers or not), we did see a weak trend in the plot of the average difference in the number of water molecules between the enzyme−PMP complex and the enzyme−external aldimine complex against the experimental yield (Figure S17). The trend is weak, but it might be worth considering in further studies because water displacement upon substrate binding may contribute to a larger energy barrier that is not accounted for in the Rosetta calculations.[53]

Crystal Structures Confirm Local Changes that Create Space. To further examine the structural basis of the activity with bulky amines and the accuracy of the Rosetta predictions, we determined crystal structures of the *Pj*TA-R6 + W58G and *Pj*TA-R6 + W58M + F86L + R417L variants. Crystallization conditions were as reported earlier.[32] Only structures with the PLP- or PMP-bound enzyme were obtained; attempts to obtain structures of *Pj*TA-R6 variants with bound external aldimines by briefly soaking crystals with substrates failed. The crystal structures for the two best variants were refined to 1.7 Å resolution with an *R*-factor of 0.173 (R_{free} = 0.191) for *Pj*TA-R6 + W58G and to 1.9 Å resolution with an *R*-factor of 0.177 (R_{free} = 0.207) for *Pj*TA-R6 + W58M + F86L + R417L (Table S3).

The *Pj*TA-R6 + W58G structure contains the PLP cofactor as internal aldimine with PLP covalently linked to Lys287, while the *Pj*TA-R6 + W58M + F86L + R417L structure contains PMP as a result of the soaking with **1b**. Similar to what was found in previous work,[19] the inserted mutations did not affect the overall backbone conformation of these *Pj*TA-R6 mutants in comparison to the *Pj*TA-R6 structure. All mutated residues showed well-defined electron density, allowing unambiguous assignment of their side chain conformations. The *Pj*TA-R6-W58G crystal structure was in agreement with the Rosetta-predicted structure (RMSD = 0.31 Å) and showed

https://doi.org/10.1021/acscatal.1c02053
ACS Catal. 2021, 11, 10733−10747

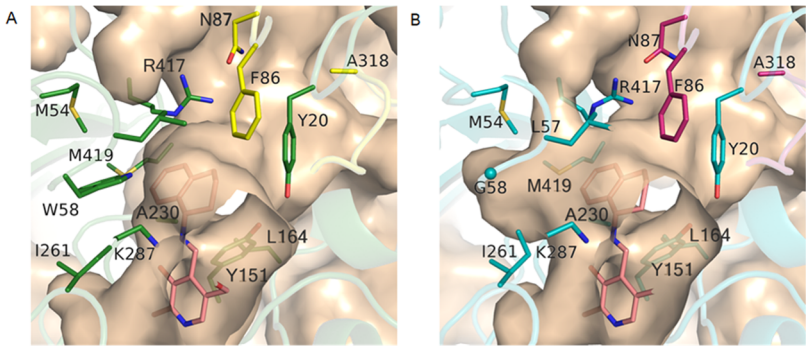

Figure 3. Effect of mutations on the active site. (A) Crystal structures of *Pj*TA-R6 (green for chain A and yellow for chain B) and (B) crystal structure of variant *Pj*TA-R6 + W58G (cyan for chain A and magenta for chain B). In both structures, intermediate **3EA** (pink) was modeled in the active site. The mutant shows an increase in the pocket volume for better accommodation of the substrate, which does not fit in *Pj*TA-R6 due to steric hindrance by Trp58. Mutation W58G greatly increases the solvent/protein contact area, which is shown as the surface (wheat).

no deviations from the *Pj*TA-R6 structure beyond the affected residues (Figure 3). Residue Trp58 is located deep in each subunit, above Lys287 and the PLP cofactor, and participates in the formation of the large binding pocket. By enlarging this pocket, mutation W58G contributes to an increase in the active site volume from 669 Å^3 in *Pj*TA-R6 to 768 Å^3 in the *Pj*TA-R6 + W58G variant, as calculated with PyVOL[54] (PLP-omitted). This reduces the steric hindrance that interferes with the binding of bulky aromatic substrates. The mutation thus facilitates accommodation of the bicyclic structure of the external aldimine formed with compound **3a**.

The *Pj*TA-R6 + W58M + F86L + R417L structure is also in agreement with the Rosetta prediction (RMSD = 0.32 Å), with negligible differences in side chain orientations (not shown). The mutations increased the active site volume (PLP omitted) from 669 Å^3 to 1187 Å^3. Superimposition of the crystal structure with Rosetta-docked poses for **1EA** showed that the substrate's phenyl ring is oriented toward the additional space in the large binding pocket obtained by replacement of Trp58 with a methionine. The propyl group is placed in the small binding pocket, which shows a slight increase in volume due to mutation F86L (Figure 4C). Mutation R417L further increases the active site volume by removing a constriction to the large binding pocket (Figure 4D). Thus, the W58M, F86L, and R417L mutations reshape the active site and reduce steric hindrance, which is necessary for accommodating intermediate **1EA** and enables amine synthesis.

Yields in Amine Synthesis. In agreement with the purpose of the computational design work, the designed mutants gave higher yields of amines **1b**−**6b** in IPA-driven transamination reactions than *Pj*TA-R6. However, yields were still modest in most cases. For example, only up to 29% yield was achieved in the synthesis of **5b** (Table 1). Reaction progress curves showed that under standard conditions (Scheme 2), accumulation of amine in the reaction mixtures did not increase after 24 h even for the best substrate−mutant combinations (Figure 5A). Furthermore, even over the first 1−4 h reaction time, amination activities were lower than expected from kinetic parameters determined under initial rate conditions (Table 2).

To identify the cause of partial conversion and low reaction rates and to find possible remedies, different measures were examined. We tested if improvement of yield could be achieved by extending reaction times after addition of fresh enzyme (1 mg), PLP (0.5 mM) or IPA (0.5 M). Also doubling the amount of enzyme added at the beginning and removing

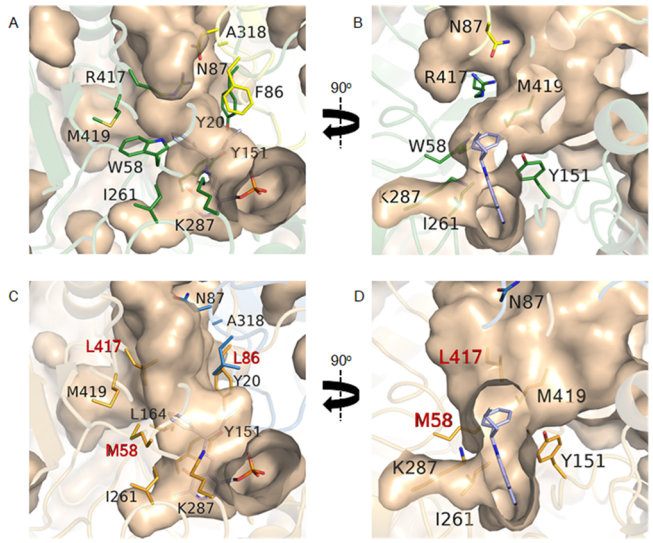

Figure 4. Effect of mutations on the active site. (A,B) Crystal structure of *Pj*TA-R6 (green, subunit A; yellow, subunit B) with the external aldimine intermediate **1EA** (light blue) modeled in the active site. The protein/solvent contact area is shown as the surface (wheat). (B) Side view of the *Pj*TA-R6 active site, rotated by 90° along the y axis, highlighting the R417 side chain that constricts the large binding pocket. (C,D) Active site of the variant *Pj*TA-R6 + W58M + F86L + R417L crystal structure (orange, subunit A; blue, subunit B; mutated residues are labeled in red), with the external aldimine intermediate **1EA** modeled inside shown in the same orientation as in panel (A) The active site volume increases due to mutations W58M and F86L. The protein/solvent contact area is shown as the surface (wheat). (D) Side view of panel (C), rotated by 90° along the y axis, showing the drastic effect of mutation R417L on the shape of the active site.

acetone by performing the reactions under low air pressure (40 kPa) during the first 24 h incubation time were attempted. However, neither of these measures had an effect on the yield.

The pH of the reaction mixtures remained constant. In contrast, when ketones (20 mM) were added again after 24 h reaction time, production of amines continued with all six substrates (Figure 5B, Table 2). The increase in amine product concentration after ketone addition suggests that the 24 h reactions had reached thermodynamic equilibrium.[55] To examine this, the apparent reaction quotient (K_Q) was calculated at 24 h and 48 h by eq 1

https://doi.org/10.1021/acscatal.1c02053
ACS Catal. 2021, 11, 10733−10747

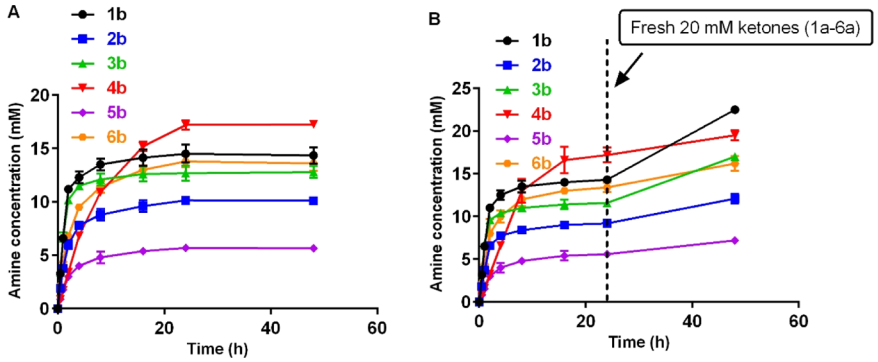

Figure 5. Production of six bulky amines (**1b**−**6b**) each by their best variant. Reaction conditions: 20 mM ketones (**1a**−**6a**), 1 M IPA, 0.5 mM PLP, 20% DMSO (2% DMSO in the case of **2a** and 15% DMSO in the case of **3a**), 1 mg/mL of enzyme, and 50 mM potassium phosphate buffer, pH 8.0. (A) The reactions were carried out for 48 h. (B) Same as in panel (A), but after 24 h reaction time, 20 mM ketone (**1a**−**6a**) was added. The reactions were continued up to 48 h. Error bars indicate individual values of duplicate assays. Data in panels (A) and (B) are from separate experiments.

Table 2. Catalytic Activities and Apparent Equilibria in the Synthesis of Amines (1b−6b)

reaction	best mutant	activity (U/mg)[a]	K_M (**1a**−**6a**) (mM)[b]	k_{cat} (**1a**−**6a**) (s^{-1})	k_{cat}/K_M (**1a**−**6a**) (mM^{-1} s^{-1})	yield at 24 h (%)[c]	yield at 48 h (%)	K_Q at 24 h	K_Q at 48 h
1a → **1b**	W58M + F86L + R417L (8)	0.12	1.5 ± 0.3	2.5 ± 0.2	1.8 ± 0.5	72 ± 1	56 ± 1	(3.6 ± 0.3) × 10^{-2}	(2.9 ± 0.1) × 10^{-2}
2a → **2b**	W58G (2)	0.062	1.6 ± 0.1	1.2 ± 0.02	0.8 ± 0.1	46 ± 1	30 ± 1	(0.8 ± 0.04) × 10^{-2}	(0.53 ± 0.04) × 10^{-2}
3a → **3b**	W58G (2)	0.11	0.6 ± 0.1	2 ± 0.03	3.4 ± 0.6	58 ± 2	43 ± 1	(1.6 ± 0.1) × 10^{-2}	(1.3 ± 0.1) × 10^{-2}
4a → **4b**	W58G (2)	0.027	4.4 ± 1.3	0.6 ± 0.1	0.2 ± 0.1	86 ± 3	49 ± 1	(12±3) ± 10^{-2}	(1.9 ± 0.1) × 10^{-2}
5a → **5b**	W58G (2)	0.027	4.6 ± 1.1	0.5 ± 0.01	0.1 ± 0.03	28 ± 1	18 ± 1	(0.22 ± 0.02) × 10^{-2}	(0.16 ± 0.01) × 10^{-2}
6a → **6b**	W58G (2)	0.073	3.6 ± 0.5	1.5 ± 0.02	0.5 ± 0.1	67 ± 2	41 ± 2	(2.8 ± 0.3) × 10^{-2}	(1.1 ± 0.1) × 10^{-2}

[a]Rates of amine production calculated over 0−1 h in Figure 5. 1 U corresponds to 1 μmol amine synthesis per min. [b]Kinetic parameters were determined by measuring initial rates of ketone depletion at varying concentrations of **1a**−**6a**. See the Materials and Methods for details. [c]Yields were calculated from the data shown in Figure 5B.

$$K_Q = \frac{[Am] \times [Ac]}{[K] \times [IPA]} \quad (1)$$

here, [Am] and [Ac] are the concentrations of amine and acetone, respectively, and [K] and [IPA] are the remaining concentrations of ketone and IPA, respectively. $[IPA]_0$ and $[K]_0$ are the added concentrations of IPA and ketones, respectively. K_Q values were calculated assuming [Ac] = [Am], $[IPA] = [IPA]_0 - [Am]$, and $[K] = [K]_0 - [Am]$. Since K_Q values at 24 h were higher than at 48 h (Table 2), only the former can represent equilibrium. Possibly, the enzyme loses activity in the 24−48 h interval, where the enzyme is exposed to a higher concentration (>20 mM) of the substrate. The results suggest that the 24 h yields reported in Table 1 for each substrate are not limited by catalytic activity but by the reaction mixtures approaching thermodynamic equilibrium.

DISCUSSION

The aim of this work was to explore the use of computational design with the Rosetta search algorithm for broadening the substrate scope of a transaminase. For this, we used *Pj*TA-R6 as the template because its engineered stability should result in high mutability.[32] The protocol avoided multiple iterations and manual selection of mutations by employing Rosetta enzyme design to obtain, in a single step, variants that catalyze amination of structurally demanding ketones. The presented methodology for broadening the substrate scope showed a high hit rate (68 out of 70 designs were successful) and good predictive power (Figure 1). The screening framework is computationally inexpensive (~2 CPU hours per enzyme variant using the HP workstation Z4 with an Intel Xeon W-2135 processor) and can easily be parallelized using multiple cores for high-throughput screening. Another attractive feature of the protocol is that combinations of mutations can be found using the Rosetta search algorithm, without the need to preselect them by rational inspection; only the search space needs to be defined. Other useful methodologies for predicting the catalytic potential of ω-TA variants (using a different intermediate) are computationally more expensive (*e.g.*, ~60 CPU hours per enzyme variant in the methodology described by Voss *et al.*[17]) or make use of coarser categorizations such as active *vs* inactive in the work of Sirin *et al.*[18] and high- *vs* low-reactivity grouping used by Han *et al.*[21] A study in which the activity toward 2-acetylbiphenyl ketone was engineered in *Vf*TA followed an approach in which mutations were added in a stepwise manner, without predicting activity for a large number of variants as a ranking tool.[20]

We chose the external aldimine as the ligand for the docking calculations because its conversion to the geminal diamine intermediate in the amine synthesis half-reaction involves a high-energy transition state.[19] Thus, we hypothesized that mutations that increase the stability of the external aldimine complex would have an observable effect on product formation.[37] An added advantage of using a ligand covalently bound to a rigid cofactor is that the position of the reactive atom (C_α) is known beforehand, which reduces both the docking search space and the number of variants that need to be screened to find a good mutant. Although the methodology described in this paper shows promising results for engineering the ω-TA activity, special attention must be paid to the identity

https://doi.org/10.1021/acscatal.1c02053
ACS Catal. 2021, 11, 10733−10747

of the substrates. The selected substrates are highly hydrophobic, which means modest direct participation from water molecules, which are typically deleted before docking. The substrates are also rigid, which, on one hand, further reduced the necessary search space and, on the other hand, made finding better variants more challenging. For substrates with high flexibility and high hydrogen-bonding potential, attention should be paid to both correct modeling of implicit or explicit water and including a good diversity of rotamers in the search space. However, this remains a serious challenge, especially due to the complexity of describing the behavior of water molecules.[56]

The design algorithm repeatedly suggested the replacement of Trp58 and Phe86 of *Pj*TA-R6 to smaller hydrophobic residues (Table 1). In view of the sequence similarities of *Vf*TA (PDB 4E3Q, 41% identity with *Pj*TA-R6), *Cv*TA (PDB 4A6T, 40% identity with *Pj*TA-R6), and ω-TA from *Ochrobactrum anthropi* (*Oa*TA, PDB 5GHF, 64% identity with *Pj*TA-R6), it is not surprising that the equivalent positions also strongly influenced activity when tested in these enzymes. The best variant of *Oa*TA possessed mutation W58A and displayed a 10^5-fold higher activity in the synthesis of **1b** than its parent, that is, 90 mU/mg.[21] Although the curves in Figure 5 indicate that amine synthesis rates drop during conversion, the initial rates of amine formation we summarize in Table 2 are higher or comparable to this value.

In *Oa*TA variants designed for **2a** and **3a**, mutation W58L relieved steric hindrance in the large binding pocket and gave a 760-fold increase in activity with **2a** (3 mU/mg) and 210-fold increase in activity with **3a** (0.7 mU/mg) compared to the parent.[23] Replacing Trp58 of *Oa*TA also promoted activity with other aliphatic and aromatic ketones, as seen with mutants W58L and W58A.[23,57] In *Vf*TA, the corresponding Trp57 was mutated to Phe or Cys in several designs for the synthesis of hydrophobic bulky amines.[15,20] In the redesign of *Vf*TA for asymmetric synthesis of (1*S*)-1-(1,1′-biphenyl-2-yl)ethanamine, the best variant-containing mutation W57F exhibited 1716-fold higher activity in comparison to the wild-type *Vf*TA.[20] Mutation W57G was beneficial for the activity of *Vf*TA toward different aliphatic amines,[58] while W57F gave improved activity with different aliphatic aldehydes and (*R*)-ethyl 5-methyl 3-oxooctanoate.[18,59,60] The corresponding position in *Cv*TA is Trp60, and mutation W60C improved the activity in the deamination of (*S*)-1-phenylethylamine and the amination of a series of ketones.[61] ω-TA mutants in which the position equivalent to Phe86 of *Pj*TA is mutated have been reported as well. Phe86 flanks the small binding pocket and was mutated to Leu to produce several variants of *Cv*TA (F88L) and *Vf*TA (F85L) that have higher activity with **1a** and gave higher yield of **1b**.[17,33] Replacement of Phe86 to the smaller Leu was enough to create room for the propyl group of **1b** in the small binding pocket. When *Vf*TA was engineered to produce **1b**, the best variant-containing mutation F85L gave 53% yield. Similarly, the best variant of *Cv*TA possessed the corresponding mutation F88L and exhibited 99% conversion in the synthesis of **1b**. Other small residues that improved activity in the synthesis of bulky amines when replacing Phe86 are Ala[11,18,60] and Val.[15]

The computational approach presented in this work avoids multiple design iterations and instead uses the Rosetta energy function in a single dock-and-design step. Rosetta found solutions that overlap with rational design approaches, pointing at the conserved Trp and Phe residues in the large and small binding pocket, respectively, as hotspots for selectivity engineering of the well-studied fold type I ω-TAs. The results show that it is possible to rapidly design transaminase variants with improved activity in the production of bulky amines. The structures predicted by Rosetta design calculations are in agreement with experimental 3D structures as determined by protein crystallography and explain the observed changes in activity. We advocate that active site redesign by covalent docking of external aldimines with simultaneous sequence optimization offers a cheap and straightforward design methodology that can be applied to broaden the substrate scope of transaminases.

■ ASSOCIATED CONTENT

Supporting Information

The Supporting Information is available free of charge at https://pubs.acs.org/doi/10.1021/acscatal.1c02053.

Substrate and intermediate structures, experimental details, chromatograms, docking structures, description of libraries, results of MD simulations, and crystallographic data (PDF)

■ AUTHOR INFORMATION

Corresponding Author

Dick B. Janssen − *Biotransformation and Biocatalysis, Groningen Biomolecular Sciences and Biotechnology Institute (GBB), University of Groningen, AG Groningen 9747 Groningen, The Netherlands;* orcid.org/0000-0002-0834-2043; Email: d.b.janssen@rug.nl

Authors

Qinglong Meng − *Biotransformation and Biocatalysis, Groningen Biomolecular Sciences and Biotechnology Institute (GBB), University of Groningen, AG Groningen 9747 Groningen, The Netherlands*

Carlos Ramírez-Palacios − *Biotransformation and Biocatalysis, Groningen Biomolecular Sciences and Biotechnology Institute (GBB), University of Groningen, AG Groningen 9747 Groningen, The Netherlands; Molecular Dynamics, Groningen Biomolecular Sciences and Biotechnology Institute (GBB), University of Groningen, AG Groningen 9747 Groningen, The Netherlands;* orcid.org/0000-0003-2724-0760

Nikolas Capra − *Biotransformation and Biocatalysis, Groningen Biomolecular Sciences and Biotechnology Institute (GBB), University of Groningen, AG Groningen 9747 Groningen, The Netherlands*

Mattijs E. Hooghwinkel − *Biotransformation and Biocatalysis, Groningen Biomolecular Sciences and Biotechnology Institute (GBB), University of Groningen, AG Groningen 9747 Groningen, The Netherlands*

Sebastian Thallmair − *Molecular Dynamics, Groningen Biomolecular Sciences and Biotechnology Institute (GBB), University of Groningen, AG Groningen 9747 Groningen, The Netherlands; Frankfurt Institute for Advanced Studies, Frankfurt am Main 60438, Germany*

Henriëtte J. Rozeboom − *Biotransformation and Biocatalysis, Groningen Biomolecular Sciences and Biotechnology Institute (GBB), University of Groningen, AG Groningen 9747 Groningen, The Netherlands*

Andy-Mark W. H. Thunnissen − *Biotransformation and Biocatalysis, Groningen Biomolecular Sciences and*

Biotechnology Institute (GBB), University of Groningen, AG Groningen 9747 Groningen, The Netherlands; orcid.org/0000-0002-1915-9850

Hein J. Wijma − *Biotransformation and Biocatalysis, Groningen Biomolecular Sciences and Biotechnology Institute (GBB), University of Groningen, AG Groningen 9747 Groningen, The Netherlands;* orcid.org/0000-0003-0891-6972

Siewert J. Marrink − *Molecular Dynamics, Groningen Biomolecular Sciences and Biotechnology Institute (GBB), University of Groningen, AG Groningen 9747 Groningen, The Netherlands;* orcid.org/0000-0001-8423-5277

Complete contact information is available at: https://pubs.acs.org/10.1021/acscatal.1c02053

Author Contributions

Q.M. and C.R.-P. contributed equally. Q.M. constructed mutants and performed the biocatalytic experiments. C.R.-P. performed the computational work. N.C., H.J.R., and A-M.W.H.T. solved the crystal structures. M.E.H. contributed to biocatalytic experiments. All authors discussed the results. Q.M., C.R.-P., and N.C. wrote the manuscript. D.B.J., S.J.M., H.J.W., and S.T. revised the manuscript. D.B.J. supervised the project.

Notes

The authors declare no competing financial interest.

■ ACKNOWLEDGMENTS

Q.M. thanks the China Scholarship Council for a Ph.D. fellowship. C.R.P. thanks CONACYT for the doctoral fellowship. Part of this project has received funding from the European Union's Horizon 2020 Programme (Marie Curie Actions-ITN ES-Cat) under GA no. 722610, which supported N.C. The research of H.J.W. was supported by the Dutch Ministry of Economic Affairs through BE-Basic, grant FS02.005. We thank the Center for Information Technology of the University of Groningen for providing access to the Peregrine high-performance computing cluster. We thank the staff of Diamond Light Source at Oxford for the excellent support and beamtime allocation.

■ ABBREVIATIONS

ω-TA, ω-transaminase; PLP, pyridoxal 5-phosphate; PMP, pyridoxamine 5-phosphate; *Pj*TA-R6, stabilized ω-TA from *Pseudomonas jessenii*; IPA, isopropylamine; *Cv*TA, ω-TA from *Chromobacterium violaceum*; *Vf*TA, ω-TA from *Vibrio fluvialis*; *Oa*TA, ω-TA from *Ochrobactrum anthropi*; dRFU/dT, change in fluorescence *versus* temperature

■ REFERENCES

(1) Kelly, S. A.; Pohle, S.; Wharry, S.; Mix, S.; Allen, C. C. R.; Moody, T. S.; Gilmore, B. F. Application of ω-Transaminases in the Pharmaceutical Industry. *Chem. Rev.* **2018**, *118*, 349−367.

(2) Eliot, A. C.; Kirsch, J. F. Pyridoxal Phosphate Enzymes: Mechanistic, Structural, and Evolutionary Considerations. *Annu. Rev. Biochem.* **2004**, *73*, 383−415.

(3) Koszelewski, D.; Tauber, K.; Faber, K.; Kroutil, W. ω-Transaminases for the synthesis of non-racemic α-chiral primary amines. *Trends Biotechnol.* **2010**, *28*, 324−332.

(4) Mathew, S.; Yun, H. ω-Transaminases for the Production of Optically Pure Amines and Unnatural Amino Acids. *ACS Catal.* **2012**, *2*, 993−1001.

(5) Gomm, A.; O'Reilly, E. Transaminases for Chiral Amine Synthesis. *Curr. Opin. Chem. Biol.* **2018**, *43*, 106−112.

(6) Bornscheuer, U. T.; Huisman, G. W.; Kazlauskas, R. J.; Lutz, S.; Moore, J. C.; Robins, K. Engineering the Third Wave of Biocatalysis. *Nature* **2012**, *485*, 185−194.

(7) Slabu, I.; Galman, J. L.; Lloyd, R. C.; Turner, N. J. Discovery, Engineering, and Synthetic Application of Transaminase Biocatalysts. *ACS Catal.* **2017**, *7*, 8263−8284.

(8) Savile, C. K.; Janey, J. M.; Mundorff, E. C.; Moore, J. C.; Tam, S.; Jarvis, W. R.; Colbeck, J. C.; Krebber, A.; Fleitz, F. J.; Brands, J.; Devine, P. N.; Huisman, G. W.; Hughes, G. J. Biocatalytic Asymmetric Synthesis of Chiral Amines from Ketones Applied to Sitagliptin Manufacture. *Science* **2010**, *329*, 305−309.

(9) Weiß, M. S.; Pavlidis, I. V.; Spurr, P.; Hanlon, S. P.; Wirz, B.; Iding, H.; Bornscheuer, U. T. Protein-Engineering of an Amine Transaminase for the Stereoselective Synthesis of a Pharmaceutically Relevant Bicyclic Amine. *Org. Biomol. Chem.* **2016**, *14*, 10249−10254.

(10) Guo, F.; Berglund, P. Transaminase Biocatalysis: Optimization and Application. *Green Chem.* **2017**, *19*, 333−360.

(11) Land, H.; Ruggieri, F.; Szekrenyi, A.; Fessner, W. D.; Berglund, P. Engineering the Active Site of an (*S*)-Selective Amine Transaminase for Acceptance of Doubly Bulky Primary Amines. *Adv. Synth. Catal.* **2020**, *362*, 812−821.

(12) Pavlidis, I. V.; Weiß, M. S.; Genz, M.; Spurr, P.; Hanlon, S. P.; Wirz, B.; Iding, H.; Bornscheuer, U. T. Identification of (*S*)-Selective Transaminases for the Asymmetric Synthesis of Bulky Chiral Amines. *Nat. Chem.* **2016**, *8*, 1076−1082.

(13) Weiß, M. S.; Pavlidis, I. V.; Spurr, P.; Hanlon, S. P.; Wirz, B.; Iding, H.; Bornscheuer, U. T. Amine Transaminase Engineering for Spatially Bulky Substrate Acceptance. *ChemBioChem* **2017**, *18*, 1022−1026.

(14) Kuipers, R. K.; Joosten, H. J.; Van Berkel, W. J. H.; Leferink, N. G. H.; Rooijen, E.; Ittmann, E.; Van Zimmeren, F.; Jochens, H.; Bornscheuer, U.; Vriend, G.; Martins Dos Santos, V. A. P.; Schaap, P. J. 3DM: Systematic Analysis of Heterogeneous Superfamily Data to Discover Protein Functionalities. *Proteins: Struct., Funct., Bioinf.* **2010**, *78*, 2101−2113.

(15) Genz, M.; Melse, O.; Schmidt, S.; Vickers, C.; Dörr, M.; van den Bergh, T.; Joosten, H.-J.; Bornscheuer, U. T. Engineering the Amine Transaminase from *Vibrio fluvialis* towards Branched-Chain Substrates. *ChemCatChem* **2016**, *8*, 3199−3202.

(16) Kiss, G.; Çelebi-Ölçüm, N.; Moretti, R.; Baker, D.; Houk, K. N. Computational Enzyme Design. *Angew. Chem., Int. Ed.* **2013**, *52*, 5700−5725.

(17) Voss, M.; Das, D.; Genz, M.; Kumar, A.; Kulkarni, N.; Kustosz, J.; Kumar, P.; Bornscheuer, U. T.; Höhne, M. In Silico Based Engineering Approach to Improve Transaminases for the Conversion of Bulky Substrates. *ACS Catal.* **2018**, *8*, 11524−11533.

(18) Sirin, S.; Kumar, R.; Martinez, C.; Karmilowicz, M. J.; Ghosh, P.; Abramov, Y. A.; Martin, V.; Sherman, W. A Computational Approach to Enzyme Design: Predicting ω-Aminotransferase Catalytic Activity Using Docking and MM-GBSA Scoring. *J. Chem. Inf. Model.* **2014**, *54*, 2334−2346.

(19) Cassimjee, K. E.; Manta, B.; Himo, F. A quantum chemical study of the ω-transaminase reaction mechanism. *Org. Biomol. Chem.* **2015**, *13*, 8453−8464.

(20) Dourado, D. F. A. R.; Pohle, S.; Carvalho, A. T. P.; Dheeman, D. S.; Caswell, J. M.; Skvortsov, T.; Miskelly, I.; Brown, R. T.; Quinn, D. J.; Allen, C. C. R.; Kulakov, L.; Huang, M.; Moody, T. S. Rational Design of a (S)-Selective-Transaminase for Asymmetric Synthesis of (1S)-1-(1,1′-biphenyl-2-yl)ethanamine. *ACS Catal.* **2016**, *6*, 7749−7759.

(21) Han, S.-W.; Kim, J.; Cho, H.-S.; Shin, J.-S. Active Site Engineering of ω-Transaminase Guided by Docking Orientation Analysis and Virtual Activity Screening. *ACS Catal.* **2017**, *7*, 3752−3762.

(22) Han, S.-W.; Park, E.-S.; Dong, J.-Y.; Shin, J.-S. Expanding Substrate Specificity of ω-Transaminase by Rational Remodeling of a

Large Substrate-Binding Pocket. *Adv. Synth. Catal.* **2015**, *357*, 2712−2720.
(23) Han, S.-W.; Park, E.-S.; Dong, J.-Y.; Shin, J.-S. Mechanism-Guided Engineering of ω-Transaminase to Accelerate Reductive Amination of Ketones. *Adv. Synth. Catal.* **2015**, *357*, 1732−1740.
(24) Binter, A.; Oberdorfer, G.; Hofzumahaus, S.; Nerstheimer, S.; Altenbacher, G.; Gruber, K.; Macheroux, P. Characterization of the PLP-Dependent Aminotransferase NikK from *Streptomyces tendae* and Its Putative Role in Nikkomycin Biosynthesis. *FEBS J.* **2011**, *278*, 4122−4135.
(25) Bolon, D. N.; Mayo, S. L. Enzyme-like Proteins by Computational Design. *Proc. Natl. Acad. Sci. U.S.A.* **2001**, *98*, 14274−14279.
(26) Richter, F.; Leaver-Fay, A.; Khare, S. D.; Bjelic, S.; Baker, D. De Novo Enzyme Design Using Rosetta3. *PLoS One* **2011**, *6*, No. e19230.
(27) Gordon, S. R.; Stanley, E. J.; Wolf, S.; Toland, A.; Wu, S. J.; Hadidi, D.; Mills, J. H.; Baker, D.; Pultz, I. S.; Siegel, J. B. Computational Design of an α-Gliadin Peptidase. *J. Am. Chem. Soc.* **2012**, *134*, 20513−20520.
(28) Privett, H. K.; Kiss, G.; Lee, T. M.; Blomberg, R.; Chica, R. A.; Thomas, L. M.; Hilvert, D.; Houk, K. N.; Mayo, S. L. Iterative Approach to Computational Enzyme Design. *Proc. Natl. Acad. Sci. U.S.A.* **2012**, *109*, 3790−3795.
(29) Das, R.; Baker, D. Macromolecular Modeling with Rosetta. *Annu. Rev. Biochem.* **2008**, *77*, 363−382.
(30) Wijma, H. J.; Floor, R. J.; Bjelic, S.; Marrink, S. J.; Baker, D.; Janssen, D. B. Enantioselective Enzymes by Computational Design and in Silico Screening. *Angew. Chem., Int. Ed.* **2015**, *54*, 3726−3730.
(31) Morin, A.; Meiler, J.; Mizoue, L. S. Computational Design of Protein-Ligand Interfaces: Potential in Therapeutic Development. *Trends Biotechnol.* **2011**, *29*, 159−166.
(32) Meng, Q.; Capra, N.; Palacio, C. M.; Lanfranchi, E.; Otzen, M.; Van Schie, L. Z.; Rozeboom, H. J.; Thunnissen, A.-M. W. H.; Wijma, H. J.; Janssen, D. B. Robust ω-Transaminases by Computational Stabilization of the Subunit Interface. *ACS Catal.* **2020**, *10*, 2915−2928.
(33) Nobili, A.; Steffen-Munsberg, F.; Kohls, H.; Trentin, I.; Schulzke, C.; Höhne, M.; Bornscheuer, U. T. Engineering the Active Site of the Amine Transaminase from *Vibrio fluvialis* for the Asymmetric Synthesis of Aryl-Alkyl Amines and Amino Alcohols. *ChemCatChem* **2015**, *7*, 757−760.
(34) Telzerow, A.; Paris, J.; Håkansson, M.; González-Sabín, J.; Ríos-Lombardía, N.; Schürmann, M.; Gröger, H.; Morís, F.; Kourist, R.; Schwab, H.; Steiner, K. Amine Transaminase from Exophiala Xenobiotica-Crystal Structure and Engineering of a Fold IV Transaminase that Naturally Converts Biaryl Ketones. *ACS Catal.* **2019**, *9*, 1140−1148.
(35) Pressnitz, D.; Fuchs, C. S.; Sattler, J. H.; Knaus, T.; Macheroux, P.; Mutti, F. G.; Kroutil, W. Asymmetric Amination of Tetralone and Chromanone Derivatives Employing ω-Transaminases. *ACS Catal.* **2013**, *3*, 555−559.
(36) Calvelage, S.; Dörr, M.; Höhne, M.; Bornscheuer, U. T. A Systematic Analysis of the Substrate Scope of (*S*)- and (*R*)-Selective Amine Transaminases. *Adv. Synth. Catal.* **2017**, *359*, 4235−4243.
(37) Dong, L.; Meng, Q.; Ramírez-Palacios, C.; Wijma, H. J.; Marrink, S. J.; Janssen, D. B. Asymmetric Synthesis of Optically Pure Aliphatic Amines with an Engineered Robust ω-Transaminase. *Catalysts* **2020**, *10*, 1310.
(38) Krieger, E.; Dunbrack, R. L.; Hooft, R. W. W.; Krieger, B. Assignment of Protonation States in Proteins and Ligands: Combining pKa Prediction with Hydrogen Bonding Network Optimization. *Methods Mol. Biol.* **2012**, *819*, 405−421.
(39) Klamt, A. Conductor-like Screening Model for Real Solvents: A New Approach to the Quantitative Calculation of Solvation Phenomena. *J. Phys. Chem.* **1995**, *99*, 2224−2235.
(40) Jakalian, A.; Jack, D. B.; Bayly, C. I. Fast, Efficient Generation of High-Quality Atomic Charges. AM1-BCC Model: II. Parameterization and Validation. *J. Comput. Chem.* **2002**, *23*, 1623−1641.
(41) Ericsson, U. B.; Hallberg, B. M.; DeTitta, G. T.; Dekker, N.; Nordlund, P. Thermofluor-Based High-Throughput Stability Optimization of Proteins for Structural Studies. *Anal. Biochem.* **2006**, *357*, 289−298.
(42) Boivin, S.; Kozak, S.; Meijers, R. Optimization of Protein Purification and Characterization Using Thermofluor Screens. *Protein Expression Purif.* **2013**, *91*, 192−206.
(43) Winter, G.; Waterman, D. G.; Parkhurst, J. M.; Brewster, A. S.; Gildea, R. J.; Gerstel, M.; Fuentes-Montero, L.; Vollmar, M.; Michels-Clark, T.; Young, I. D.; Sauter, N. K.; Evans, G. DIALS: Implementation and Evaluation of a New Integration Package. *Acta Crystallogr., Sect. D: Struct. Biol.* **2018**, *74*, 85−97.
(44) Evans, P. R.; Murshudov, G. N. How Good Are My Data and What Is the Resolution? *Acta Crystallogr., Sect. D: Biol. Crystallogr.* **2013**, *69*, 1204−1214.
(45) Winn, M. D.; Ballard, C. C.; Cowtan, K. D.; Dodson, E. J.; Emsley, P.; Evans, P. R.; Keegan, R. M.; Krissinel, E. B.; Leslie, A. G. W.; McCoy, A.; McNicholas, S. J.; Murshudov, G. N.; Pannu, N. S.; Potterton, E. A.; Powell, H. R.; Read, R. J.; Vagin, A.; Wilson, K. S. Overview of the CCP4 suite and current developments. *Acta Crystallogr., Sect. D: Biol. Crystallogr.* **2011**, *67*, 235−242.
(46) Murshudov, G. N.; Skubák, P.; Lebedev, A. A.; Pannu, N. S.; Steiner, R. A.; Nicholls, R. A.; Winn, M. D.; Long, F.; Vagin, A. A. REFMAC5 for the Refinement of Macromolecular Crystal Structures. *Acta Crystallogr., Sect. D: Biol. Crystallogr.* **2011**, *67*, 355−367.
(47) Emsley, P.; Lohkamp, B.; Scott, W. G.; Cowtan, K. Features and development of Coot. *Acta Crystallogr., Sect. D: Biol. Crystallogr.* **2010**, *66*, 486−501.
(48) Lilkova, E. *The PyMOL Molecular Graphics System, Version 2.0*; Schrödinger, LLC, 2015.
(49) Jha, R. K.; Chakraborti, S.; Kern, T. L.; Fox, D. T.; Strauss, C. E. M. Rosetta Comparative Modeling for Library Design: Engineering Alternative Inducer Specificity in a Transcription Factor. *Proteins: Struct., Funct., Bioinf.* **2015**, *83*, 1327−1340.
(50) Börner, T.; Rämisch, S.; Bartsch, S.; Vogel, A.; Adlercreutz, P.; Grey, C. Three in One: Temperature, Solvent and Catalytic Stability by Engineering the Cofactor-Binding Element of Amine Transaminase. *ChemBioChem* **2017**, *18*, 1482−1486.
(51) Ladbury, J. E. Just add water! The effect of water on the specificity of protein-ligand binding sites and its potential application to drug design. *Chem. Biol.* **1996**, *3*, 973−980.
(52) Abel, R.; Young, T.; Farid, R.; Berne, B. J.; Friesner, R. A. Role of the Active-Site Solvent in the Thermodynamics of Factor Xa Ligand Binding. *J. Am. Chem. Soc.* **2008**, *130*, 2817−2831.
(53) Wahl, J.; Smieško, M. Thermodynamic Insight into the Effects of Water Displacement and Rearrangement upon Ligand Modifications Using Molecular Dynamics Simulations. *ChemMedChem* **2018**, *13*, 1325−1335.
(54) Smith, R. H. B.; Dar, A. C.; Schlessinger, A. *PyVOL: A PyMOL Plugin for Visualization, Comparison, and Volume Calculation of Drug-Binding Sites*; bioRxiv, 2019.
(55) Goldberg, R. N. Standards in Biothermodynamics. *Perspect. Sci.* **2014**, *1*, 7−14.
(56) Leman, J. K.; Weitzner, B. D.; Lewis, S. M.; Adolf-Bryfogle, J.; Alam, N.; Alford, R. F.; Aprahamian, M.; Baker, D.; Barlow, K. A.; Barth, P.; Basanta, B.; Bender, B. J.; Blacklock, K.; Bonet, J.; Boyken, S. E.; Bradley, P.; Bystroff, C.; Conway, P.; Cooper, S.; Correia, B. E.; Coventry, B.; Das, R.; De Jong, R. M.; DiMaio, F.; Dsilva, L.; Dunbrack, R.; Ford, A. S.; Frenz, B.; Fu, D. Y.; Geniesse, C.; Goldschmidt, L.; Gowthaman, R.; Gray, J. J.; Gront, D.; Guffy, S.; Horowitz, S.; Huang, P.-S.; Huber, T.; Jacobs, T. M.; Jeliazkov, J. R.; Johnson, D. K.; Kappel, K.; Karanicolas, J.; Khakzad, H.; Khar, K. R.; Khare, S. D.; Khatib, F.; Khramushin, A.; King, I. C.; Kleffner, R.; Koepnick, B.; Kortemme, T.; Kuenze, G.; Kuhlman, B.; Kuroda, D.; Labonte, J. W.; Lai, J. K.; Lapidoth, G.; Leaver-Fay, A.; Lindert, S.; Linsky, T.; London, N.; Lubin, J. H.; Lyskov, S.; Maguire, J.; Malmström, L.; Marcos, E.; Marcu, O.; Marze, N. A.; Meiler, J.; Moretti, R.; Mulligan, V. K.; Nerli, S.; Norn, C.; Ó'Conchúir, S.; Ollikainen, N.; Ovchinnikov, S.; Pacella, M. S.; Pan, X.; Park, H.;

https://doi.org/10.1021/acscatal.1c02053
ACS Catal. 2021, 11, 10733−10747

Pavlovicz, R. E.; Pethe, M.; Pierce, B. G.; Pilla, K. B.; Raveh, B.; Renfrew, P. D.; Burman, S. S. R.; Rubenstein, A.; Sauer, M. F.; Scheck, A.; Schief, W.; Schueler-Furman, O.; Sedan, Y.; Sevy, A. M.; Sgourakis, N. G.; Shi, L.; Siegel, J. B.; Silva, D.-A.; Smith, S.; Song, Y.; Stein, A.; Szegedy, M.; Teets, F. D.; Thyme, S. B.; Wang, R. Y.-R.; Watkins, A.; Zimmerman, L.; Bonneau, R. Macromolecular Modeling and Design in Rosetta: Recent Methods and Frameworks. *Nat. Methods* **2020**, *17*, 665−680.

(57) Kim, H.-G.; Han, S.-W.; Shin, J.-S. Combinatorial Mutation Analysis of ω-Transaminase to Create an Engineered Variant Capable of Asymmetric Amination of Isobutyrophenone. *Adv. Synth. Catal.* **2019**, *361*, 2594−2606.

(58) Cho, B.-K.; Park, H.-Y.; Seo, J.-H.; Kim, J.; Kang, T.-J.; Lee, B.-S.; Kim, B.-G. Redesigning the substrate specificity of ω-amino-transferase for the kinetic resolution of aliphatic chiral amines. *Biotechnol. Bioeng.* **2008**, *99*, 275−284.

(59) Genz, M.; Vickers, C.; van den Bergh, T.; Joosten, H.-J.; Dörr, M.; Höhne, M.; Bornscheuer, U. Alteration of the Donor/Acceptor Spectrum of the (*S*)-Amine Transaminase from *Vibrio fluvialis*. *Int. J. Mol. Sci.* **2015**, *16*, 26953−26963.

(60) Midelfort, K. S.; Kumar, R.; Han, S.; Karmilowicz, M. J.; McConnell, K.; Gehlhaar, D. K.; Mistry, A.; Chang, J. S.; Anderson, M.; Villalobos, A.; Minshull, J.; Govindarajan, S.; Wong, J. W. Redesigning and Characterizing the Substrate Specificity and Activity of *Vibrio fluvialis* Aminotransferase for the Synthesis of Imagabalin. *Protein Eng., Des. Sel.* **2013**, *26*, 25−33.

(61) Cassimjee, K. E.; Humble, M. S.; Land, H.; Abedi, V.; Berglund, P. Chromobacterium violaceum ω-transaminase variant Trp60Cys shows increased specificity for (S)-1-phenylethylamine and 4′-substituted acetophenones, and follows Swain-Lupton parameter-isation. *Org. Biomol. Chem.* **2012**, *10*, 5466−5470.

https://doi.org/10.1021/acscatal.1c02053
ACS Catal. 2021, 11, 10733−10747